Electronic structure and quantum criticality in $Ba(Fe_{1-x-y}Co_xMn_y)_2As_2$, an ARPES study.

E. D. L. Rienks,[1] T. Wolf,[2] K. Koepernik,[3] I. Avigo,[4] P. Hlawenka,[1] C. Lupulescu,[5] T. Arion,[6] F. Roth,[3] W. Eberhardt,[5,7] U. Bovensiepen,[4] J. Fink[3]

[1] *Helmholtz-Zentrum Berlin, Albert-Einstein-Strasse 15, 12489 Berlin, Germany*

[2] *Karlsruhe Institute of Technology, Institut für Festkörperphysik, D-76021 Karlsruhe, Germany*

[3] *Leibniz-Institute for Solid State and Materials Research Dresden, P.O.Box 270116, D-01171 Dresden, Germany*

[4] *Fakultät für Physik, Universität Duisburg-âĂŞEssen, Lotharstr. 1, D-47048 Duisburg, Germany*

[5] *Technische Universität Berlin, Institut für Optik und Atomare Physik, Strasse des 17. Juni 136, D-10623 Berlin, Germany*

[6] *Institut fÃijr Experimentalphysik, UniversitÃďt Hamburg, Luruper Chaussee 149, 22761 Hamburg, Germany*

[7] *Center for Free-Electron Laser Science / DESY, Notkestrasse 85, 22607 Hamburg, Germany*

(Dated: January 21, 2013)

We used angle-resolved photoemission spectroscopy (ARPES) and density functional theory calculations to study the electronic structure of $Ba(Fe_{1-x-y}Co_xMn_y)_2As_2$ for x=0.06 and $0 \leq y \leq 0.07$. We derive a non-rigid-band like change of the electronic structure as a function of Mn substitution and an effective doping close to one hole per Mn ion. An evaluation of the measured spectral function does not indicate a diverging effective mass or scattering rate near optimal doping. Thus the present ARPES results indicate a continuous evolution of the quasiparticle interaction and therefore question previous quantum critical scenarios.

PACS numbers: 74.70.Xa, 74.25.Jb, 74.40.Kb

In many compounds such as heavy fermion systems, doped cuprates, molecular crystals, and ferropnictides [1, 2], unconventional/high–temperature superconductivity occurs close to a point in the phase diagram where the antiferromangetic order is suppressed at zero temperature. The transition into the superconducting region can be tuned by pressure, chemical pressure, doping, or some other control parameter. Different from a temperature-driven transition, large quantum fluctuations are expected in the zero temperature phase transitions which led to the introduction of the term quantum criticality [3, 4]. Near the quantum critical point a non-Fermi-liquid behavior is detected, which is related to a diverging effective mass and scattering rate and to a disappearance of the quasiparticle spectral weight at the Fermi level. The general explanation for the deviation from a Fermi liquid behavior in this region of the phase diagram is that electrons strongly interact with collective modes related to the antiferromagnetic (AFM) order. It is supposed that the superconducting phase appearing close to the quantum critical point is due to a coupling of the charge carriers to these quantum fluctuations. This would provide a universal explanation of the pairing mechanism for unconventional superconductivity. Both quantum critical phenomena and unconventional superconductivity are major themes in current condensed matter physics.

For the iron pnictides the quantum criticality scenario has been proposed theoretically by Dai et al. [5]. Experimentally, in ferropnictides, the scheme of a quantum critical point is supported by transport and thermodynamic measurements [6–9].

Angle-resolved photoemission spectroscopy (ARPES) [10] is not only a very useful tool to determine the Fermi surface topology, but offers also the unique possibility to determine the momentum dependent spectral function which contains information on the complex self-energy $\Sigma = \Sigma' + i\Sigma''$, which is related to the mass renormalization and the scattering rate. We emphasize here that the momentum dependent ARPES data provide information on both the hot and the cold spots on the Fermi level. In the ferropnictides, the hot spots are caused by a partial nesting between hole and electron pockets, yielding the AFM order, AFM quantum fluctuations, and possibly also superconductivity. The cold spots determine the transport and thermodynamic properties. A variation of the charge carrier dynamics at different points of the Fermi level is expected due to the changes of the nesting conditions and/or the orbital

character of the Fermi surface in k-space [11].

In this Letter we report an electronic structure study of $Ba(Fe_{1-x-y}Co_xMn_y)_2As_2$ (BFCMA) by means of ARPES. We focus on a series of crystals with x=0.06 and a variable Mn substitution with $0 \leq y \leq 0.07$. For $y = 0$, T_c is close to its optimal value and close to the extrapolated zero temperature value of T_N. Thus within a quantum critical scenario we should find diverging effective masses and scattering rates. With increasing Mn substitution previous studies on the same system have detected a rapid decrease of T_c, a disappearance of superconductivity near $y = 0.02$ [12], and a T_N which reaches a maximum of 23 K at y=0.01 and disappears near y=0.03 [13]. This signals that with increasing Mn substitution one departs from a possible quantum critical point and therefore the scattering rates and the mass renormalization should be reduced.

In the most simple picture, the substitution of Fe by Mn leads to hole doping and thus one should move to a lower total electron number. However, studies on $Sr(Fe_{1-x}Mn_x)_2As_2$ indicate that the case is by far more complex [14]. Although T_N decreases with increasing Mn concentration, superconductivity does not appear which is in stark contrast to the hole doped system with K substitution on the Sr site. This discrepancy was interpreted in terms of structural modifications rather than carrier doping.

Our ARPES study on BFCMA reveals an increasing number of holes upon Mn substitution. On the other hand, the observed non-rigid-band behavior cannot explain the changes of the electronic structure by a mere charge doping. Upon Mn substitution the scattering rates and the mass renormalization do not decrease indicating that there is no pronounced coupling of spin fluctuations to the charge carriers exactly at optimal doping.

Single crystals of BFCMA were grown from the self-flux and characterized by resistivity, magnetization, specific heat, and dilatometry measurements [13]. ARPES measurements were carried out at the synchrotron radiation facility BESSY II using the UE112-PGM2a beam line and the "1^2"-ARPES end station equipped with a Scienta R8000 analyzer. The total energy resolution was 10-15 meV, while the angular resolution was 0.2°. All measurements were performed in the paramagnetic and non-superconducting range near T=30 K. For the presentation we use a coordinate system parallel to the Fe-Fe direction as in our previous ARPES study [15].

We performed density functional theory (DFT) calculations within the generalized gradient approximation (GGA) [16] using the scalar relativistic mode of the Full Potential Local Orbitial code (FPLO) [17]. The doping was simulated by constructing supercells with x=0.06 and y=0 or 0.07. For k-integration we used the tetrahedron method with 6^3 points in the full Brillouin zone of the resulting unit cells with 16 Fe(Co/Mn) positions. We constructed 4 different cells for y=0.07 with different relative Co-Mn arrangements. The As-position and lattice parameters are taken from experimental x–ray diffraction data [13].

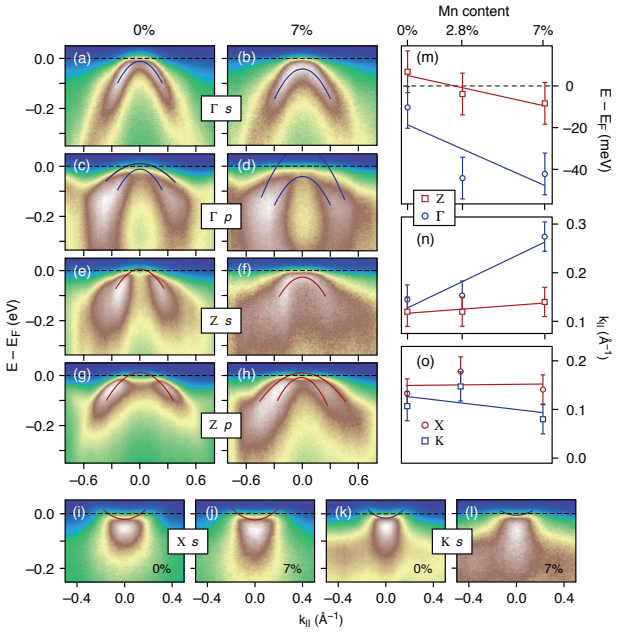

Figure 1. (color online) ARPES data of BFCMA . (a)-(l) Intensity plots as a function of binding energy and wave vectors along the k_y direction for x = 0.06 and y=0 and 0.07 near the high-symmetry points Γ, Z, X, and K. The spectra near Γ and Z are shown for s- and p-polarized photons. The red/blue lines represent parabolic bands derived from least squares fits. (m)-(o) Fermi wave vectors near high-symmetry points as a function of Mn concentration. The solid lines are least-squares fits assuming a linear dependence of k_F on y

Figure 1 (a)-(l) shows representative ARPES data of BFCMA for x=0.06 and two different Mn concentrations near high-symmetry points for s (perpendicular to k_x) and p (parallel to k_x) polarized light. The panels show intensity plots along the k_y direction as a function of binding energy. The high-symmetry points were reached by using variable photon energies as outlined in our previous studies of ferropnictides [15]. Due to matrix element effects, for s-polarization in the present geometry we detect at Γ and Z bands which have uneven symmetry relative to the scattering plane, i.e., bands having predominantly Fe 3d xz/yz orbital character forming the two inner, almost degenerate hole pockets [15, 18]. For p-polarization we detect in addition bands with xy and z^2 (even) orbital character, forming the outer hole pocket. At X and K we detect for s-polarization the electron pocket which has at that point predominantly xz/yz character, while (not shown) for p–polarization the spectral weight is rather small due to matrix element effects.

Using momentum distribution curves (MDC) we have determined the dispersion of bands which are shown in Fig. 1 by red/blue lines. The Fermi wave vectors that

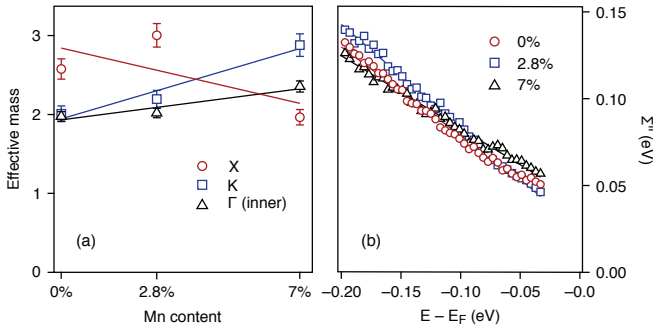

Figure 2. (color online) Effective mass and scattering rates for BFCMA as a function of Mn concentration. (a) effective mass m^*/m near three high symmetry points (b) Σ" for the inner hole pocket near the Γ point. In both panels the solid lines are derived by least-squares fits assuming a linear dependence.

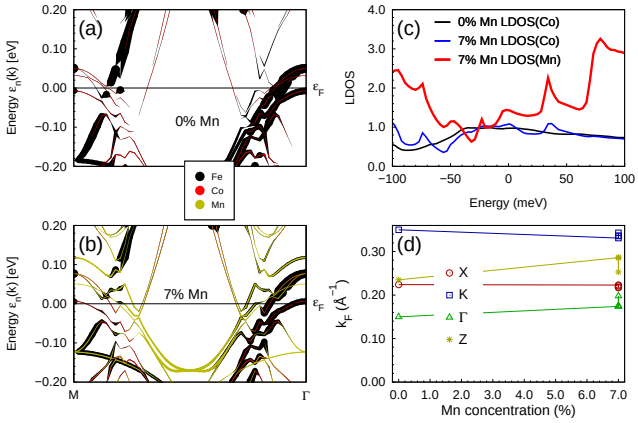

Figure 3. (color online) (a,b): unfolded band structure along M/Γ with Co and Mn impurity weights shown in medium(red) and light(yellow), respectively. Note that the gaps in the main Fe bands (black) are washed out in ensemble average. (c): local density of states (LDOS) for Co and Mn impurity bands; (d): Fermi radii for the outer hole and electron bands. Note, that there are 4 supercells/data-points for y=0.07.

can be obtained from these dispersions are presented in Fig. 1 (m)-(o). Since for x=0.06 the inner hole pockets are (almost) completely filled, we show for these pockets the energy of the band maximum relative to the Fermi level.

In Fig. 2 (a) we depict the effective mass m^*/m_b near high symmetry points as a function of Mn concentration. Here m^* is the mass derived from the measured dispersion and m_b is the mass derived from tight-binding band structure calculations [19]. Using the measured dispersion as an input for $\epsilon_k - \Sigma'$ (ϵ_k is the bare particle dispersion) in the formula for the spectral function [10] an MDC fit yields values for Σ" for the inner hole pocket along the k_y direction near Γ which are presented in Fig. 2 (b) for three different Mn concentrations.

First we discuss the fermiology as a function of Mn substitution. The k_F values presented in Fig. 1 (m)-(o) indicate that the diameter of the outer hole pocket cylinder increases. The inner hole ellipsoid around the Z point disappears near y=0.02 and therefore does not contribute significantly to the changes of the total hole count. Since also the changes of the diameter of the electron cylinder are small, the increasing diameter of the outer hole cylinder signals a total increasing hole concentration. From an evaluation of the diameter of the hole and electron cylinders, similar to that in our previous study [15], we estimate a total doping close to one hole per Mn ion.

The shift of the outer hole pocket at Γ to positive $E - E_F$-values, causing increasing k_F-values, together with a shift of the inner hole pocket to negative $E - E_F$-values indicates a non-rigid-band behavior as a function of Mn substitution similar to that derived in our ARPES study on $EuFe_2As_{2-x}P_x$ but in contrast to our results on $Ba(Fe_{1-x}Co_x)_2As_2$ [15]. Our findings support the statement of Kim et al. [14] that the electronic structure of Mn substituted $BaFe_2As_2$ is not only determined by the amount of charge but also by structural changes due to the larger ion diameter of Mn compared to Fe. These structural changes increase in particular the Fe-As distance thus leading to a different energy shift for bands having different orbital character.

The DFT results (see Fig. 3) support the non-rigid band picture given by ARPES. In order to analyse the calculated band structure we use the band unfolding technique, which removes most of the backfolded bands due to the supercells. The outer hole bands at Γ/Z move up and hence acquire a larger Fermi radius, while the inner cylinder stays almost unchanged near zero energy. The latter effect is present in 3 out of 4 y=0.07 supercells, while in the fourth cell this band moves up more significantly. The radius of the outer electron bands stays rather constant, which is partially due to the fact that this is a very steep band. The direct comparison of Fermi radii with ARPES gives only qualitative agreement, since the warping due to z–dispersion is usually more pronounced in DFT, even for the undoped compound. We observe that around Γ/Z the outer hole bands have a larger Mn impurity weight compared to the inner bands, which together with the higher Mn on–site energy may be part of the reason for the upward shift. Furthermore, we note that the Mn impurity spectral weight close to the Fermi level is enhanced as compared to the Co impurity weight (see Fig. 3 (c)), which might also be related to the relative positions of on–site energies. This Mn impurity spectral weight introduces scattering, which is detrimental to superconductivity. From this point of view back-doping with Mn is not equivalent to reducing the Co-doping, whose impurity bands tend to be further away from the Fermi level.

Next we discuss the possibility of a change of the mass renormalization as a function of the Mn concentration. We focus first on those parts of the Fermi surface which have predominantly xz/yz orbital character since according to calculations in the random-phase-approximation [11, 20] interband transitions between those bands should lead to the highest spin fluctuation susceptibilities, i.e., in particular at those hot spots quantum criticality should occur. As shown in Fig. 2 (a), the mass renormalization of the inner hole pocket and the electron pocket does not show at these hot spots a decrease which would be expected for an increasing distance to the quantum critical point. Rather at least near Γ and K a slight increase is realized. In addition, we emphasize that close to the Fermi level we do not detect a deviation from a parabolic dispersion (see Fig. 1 (a)) which could be related to a low–energy mass enhancement. This is a first indication that from our ARPES experiments we cannot conclude on the existence of a quantum critical point near optimal doping. One may argue that upon Mn substitution, we remain at the quantum critical point. Therefore we evaluated the effective masses of the same bands in $Ba(Fe_{1-x}Co_x)_2As_2$ using our previous ARPES data [15]. Also in this system the effective masses in the paramagnetic state remain constant when going from the undoped case to optimal doping and finally to the overdoped case. Thus, contrary to the de HaasâĂŞ-van Alphen measurements on $BaFe_2As_{2-x}P_x$ [8], an enhanced effective mass near optimal doping is observed neither in $Ba(Fe_{1-x}Co_x)_2As_2$ nor in BFCMA.

We expect a corresponding result for the scattering rates. As depicted in Fig. 2 (b), for the inner hole pocket $\Sigma"=\alpha+\beta E$ where $\alpha \approx 40$ meV is determined by elastic scattering due to defects, e.g. by a disordered Ba surface [21]. The coefficient $\beta \approx 0.5$ is a measure for the inelastic scattering rate related to electron-electron interaction, e.g. via a coupling to excitations of spin fluctuations. Our data on $\Sigma"$ reveal the same energy dependence for all Mn concentrations. It is remarkable that an evaluation of $\Sigma"$ of our previous $Ba(Fe_{1-x}Co_x)_2As_2$ data for x= 0 to 0.2 in the paramagnetic state yield the same α and β values, independent of the Co concentration. Thus also the scattering rates derived from our ARPES experiments on this system do not diverge at optimal doping and thus do not support a quantum critical point where a particularly large coupling of spin fluctuations to the charge carriers is expected.

One may argue that in the present ARPES experiments the temperature is too high to detect indications of quantum criticality in the pnictides. We emphasize that the strange behavior of the thermodynamic and transport properties was detected at comparable temperatures where the present information on the scattering rates was obtained.

Since the thermodynamic and the transport properties may be determined by the cold spots of the Fermi surfaces we also discuss the renormalization of these bands although there is less information available from our ARPES measurements. The outer hole pocket has predominantly xy orbital character and according to theoretical results [11, 20] the susceptibility for spin fluctuations should be considerably smaller for this band. Indeed our ARPES data show strongly reduced scattering rates for the outer hole pocket although it is difficult to evaluate exact values for β. Finally, according to the RPA calculations [11, 20], along the k_x direction there should be also a part of the electron pocket with predominantly xy orbital character which should have a lower renormalization caused by electron-electron interaction. This is indeed observed in ARPES experiments by Brouet et al. [18] where the scattering rate of the electron pocket along k_y (yz character) is about twice as large as that along the k_x direction (xy character). Thus measured scattering rates do not indicate a strong renormalization for the cold spot with xy character at optimal doping.

In the present ARPES study of BFCMA at the hot spots we do not detect a particularly strong coupling to spin fluctuations at optimal doping which is expected in a quantum critical scenarios for unconventional superconductivity. The reason for this is probably that the energy scale of the spin fluctuation excitations, coupled to the charge carriers in a dynamical nesting process is rather high compared to the energetic changes of the band structure caused by Fe substitution. This view is supported by very recent resonant inelastic x-ray scattering study in which spin excitations in the energy range 150-200 meV were detected with minor changes when going from the undoped AFM compound to the paramagnetic superconducting system [22]. In this way it is possible to understand the continuous development of the renormalization of the electronic structure in a large range of the control parameter which was also observed for the Drude scattering rates derived from optical spectroscopy [23].

In this context, it is interesting that in other systems the strange properties near a quantum critical point are often discussed in terms of a single electron model, e.g. by a band edge or a singularity in the density of states and/or changes in the topology of the Fermi surface [24]. In the ferropnictides such scenarios are possible since near optimal doping a Lifshitz transition is observed: the Fermi surface changes from a cylinder along the k_z direction to an ellipsoid around the Z point [15, 25] (see also Fig. 1 (a)-(h)). This observation may indicate the importance of this Lifshitz transition for the magnetic and the superconducting properties of pnictides.

We acknowledge funding by the DFG through the priority program SPP1458. We thank Peter Schweiss for providing x-ray diffraction data of the samples and Roman Schuster for helpful discussions.

[1] D. C. Johnston, Adv. Phys. **59**, 803 (2010).
[2] G. R. Stewart, Rev. Mod. Phys. **83**, 1589 (2011).
[3] H. v. LÃűhneysen, A. Rosch, M. Vojta, and P. WÃűlfle, Rev. Mod. Phys. **79**, 1015 (2007).
[4] P. Gegenwart, Q. Si, and F. Steglich, Nat Phys **4**, 186 (2008).
[5] J. Dai, Q. Si, J.-X. Zhu, and E. Abrahams, PNAS **106**, 4118 (2009).
[6] J.-H. Chu, J. G. Analytis, C. Kucharczyk, and I. R. Fisher, Phys. Rev. B **79**, 014506 (2009).
[7] J. Maiwald, H. S. Jeevan, and P. Gegenwart, Phys. Rev. B **85**, 024511 (2012).
[8] H. Shishido et al., Phys. Rev. Lett. **104**, 057008 (2010).
[9] C. Meingast et al., Phys. Rev. Lett. **108**, 177004 (2012).
[10] S. Hüfner, *Photoelectron Spectroscopy: Principles and Application*, Springer-Verlag, New York, 2003.
[11] P. J. Hirschfeld, M. M. Korshunov, and I. I. Mazin, Rep. Prog. Phys. **74**, 124508 (2011).
[12] J. Li et al., Solid State Commun. **152**, 671 (2012).
[13] F. Hardy, P. Adelmann, T. Wolf, H. v. LÃűhneysen, and C. Meingast, Phys. Rev. Lett. **102**, 187004 (2009), and A. Böhmer et al. (unpublished).
[14] J. S. Kim et al., Phys. Rev. B **82**, 024510 (2010).
[15] S. Thirupathaiah et al., Phys. Rev. B **84**, 014531 (2011).
[16] J. P. Perdew, K. Burke, and M. Ernzerhof, Phys. Rev. Lett. **77**, 3865 (1996).
[17] K. Koepernik and H. Eschrig, Phys. Rev. B **59**, 1743 (1999), http://www.fplo.de.
[18] V. Brouet et al., arXiv e-prints:1105.5604 (2011).
[19] M. M. Korshunov and I. Eremin, Phys. Rev. B **78**, 140509 (2008).
[20] S. Graser, T. A. Maier, P. J. Hirschfeld, and D. J. Scalapino, New J. Phys. **11**, 025016 (2009).
[21] E. van Heumen et al., Phys. Rev. Lett. **106**, 027002 (2011).
[22] K. J. Zhou et al., arXiv:1301.1289 (2013).
[23] M. Nakajima et al., Phys. Rev. B **81**, 104528 (2010).
[24] H. Pfau, R. Daou, M. Brando, and F. Steglich, Phys. Rev. B **85**, 035127 (2012).
[25] C. Liu et al., Nat Phys **6**, 419 (2010).